

Contents lists available at ScienceDirect

Petroleum Science

journal homepage: www.keaipublishing.com/en/journals/petroleum-science



Original Paper

Fluvial reservoir characterization through channel belt dimension and petrophysical analysis



Shakhawat Hossain*, Tahmidur Rahman Junayed, Naymur Rahman

Department of Geology, University of Dhaka, Dhaka, 1000, Bangladesh

ARTICLE INFO

Article history:
Received 21 August 2021
Received in revised form
13 July 2022
Accepted 26 September 2022
Available online 30 September 2022

Edited by Teng Zhu and Jia-Jia Fei

Keywords: Log motif Fluvial Channel belt dimension Seismic geomorphology Petrophysics Moragot field

ABSTRACT

The dimensions and connectivity of fluvial reservoirs vary greatly, making it challenging to characterize them using conventional approaches. In this study integrated channel belt dimension analysis from seismic geomorphology and empirical equations, well log facies, and petrophysical analysis were performed to characterize the fluvial reservoirs. The study interval consists of fluvial deposits and is divided into three reservoir zones, which are defined by four key regional markers (B, D, K, O). In these intervals, six (6) fluvial facies have been identified. Based on the log facies proportions and their stacking relationships, it is interpreted that the reservoirs in zone 1 (B to D) were deposited in a proximal reach of a meandering system, zone 2 (D to K) in a marginal marine setting, and zone 3 (K) in a distal reach of a meandering system. The dimensions of fluvial channels and channel belts were determined using empirical equations. The results were compared with the observed dimensions of fluvial channels and channel belts from the seismic horizon and stratal slices of the same intervals. Zones 1 and 3 are characterized by broad meander belts (1000-4000 m) compared to zone 2 (600-1300 m). Petrophysical analysis showed zones 1 and 3 have the better petrophysical properties compared to zone 2. Though zone 3 has the most well-developed sand bodies, the best reservoir interval is zone 1 because of its higher porosity. Although channel belt dimensions have a significant influence on reservoir connectivity, they do not seem to have control on reservoir properties. The channel belt dimensions obtained from the empirical equations and interpreted from the seismic geomorphology analysis were found to be strikingly similar. Since three-dimensional seismic data is not available everywhere and seismic imaging quality decreases with depth, empirical equations can be used to analyze fluvial reservoir parameters and their connectivity at greater depths.

© 2022 The Authors. Publishing services by Elsevier B.V. on behalf of KeAi Communications Co. Ltd. This is an open access article under the CC BY-NC-ND license (http://creativecommons.org/licenses/by-nc-nd/

4.0/).

1. Introduction

Fluvial deposits often constitute a substantial part of the basin fill. They represent some of the best hydrocarbon reservoirs and aquifers (Shanley, 2004). Characterization of fluvial stratigraphic architecture, including the complex distribution of sandy channel deposits and fine-grained overbank units, is crucial for understanding the extent, connectivity, facies, and fluid distribution within units (Allen, 1979; Allen et al., 1983; Potter, 1967; Hornung and Aigner, 1999; Raiber et al., 2012). Types and dimensions of fluvial reservoirs differ widely. Additionally, fluvial systems extend for a long distance, some of them (e.g., Makenzie river in Canada)

* Corresponding author. E-mail address: shakhawat.geo@du.ac.bd (S. Hossain). even stretch over more than 3000 km. Due to the large lateral extent, it is critical to identify the part of the reach where the reservoirs understudied were deposited. Therefore, the identification of fluvial depositional sub-domains is crucial. Several approaches can be used to study depositional settings.

Log facies analysis is a tool that can be used to identify depositional facies and depositional settings. Depositional log facies and their stacking pattern can be used to determine the depositional system. Works on modern sedimentary environments suggest vertical grain size distribution in different depositional settings have different characteristics (Amajor and Agbaire, 1989; Chow et al., 2005; Heldreich et al., 2017; Selley and Sonnenberg, 1985). While meandering rivers form a fining upward succession, prograding deltas form a coarsening upward succession. The successions show up as different trends on wireline logs. The common trends associated with depositional settings include coarsening

upward trend, showing the deltaic facies, fining upward trend, and showing the transgressive facies, boxcar gamma-ray log motif of regressive barrier bar/beach deposits (Rider, 1996). For sedimentary facies interpretation, gamma-ray log motif is most commonly used. Study of the Gamma ray log has revealed several distinct patterns that can be associated with depositional processes. If there is no core of rock present, then this is the best method for facies interpretation. By using GR log and seismic data (Kessler and Sachs. 1995), they examined the sedimentary process of sandstones in Ireland (Chow et al., 2005), studied GR log facies from nine wells in Taiwan to determine the paleo-environment of the Erchungchi "A" Member by analyzing its log trend (Cant, 1992), and suggests that clean massive sands are associated with a cylindrical trend. Typically, aeolian sands, confined fluvial channels, submarine canyon fills as a suitable environment of cylindrical/boxcar shape (Selley and Sonnenberg, 1985). They considered funnel shape in wireline logs to be related to tidal sands, grain flow fills, and prograding delta distributaries channel sedimentary environments in clastic settings (Nazeer et al., 2016; Imran et al., 2020), and further subdivided the box shape into the left boxcar and the right boxcar. A consistent trend of GR with low value is called a left boxcar. The consistent trend of GR on the right side shows the high value of GR in shale and is called the right boxcar. The right box car is indicative of a muddy tidal flat depositional environment. The bell shape is associated with the fluvial point bar, the tidal point bar, deep sea channels, detail distributaries, and the proximal deep-sea setting. In cases where the trend of fining upward is not clean and the trend of bell shape is serrated, the lithology is considered heterolithic.

Another aspect of fluvial reservoirs is the size of the channel and channel belt. Channel belt dimensions determine lateral connectivity of fluvial reservoirs, which is dependent on channel width. Seismic geomorphology and observations from outcrop are typically used to identify the architectural elements in fluvial systems (Corbett et al., 2011; Hubbard et al., 2011; Miall, 2002; Reijenstein et al., 2011; Zou et al., 2010). Some parts of the world do not have three-dimensional seismic data and have no outcrops of good quality, therefore most subsurface data analysis involves interpreting well logs. This often leads to high levels of uncertainty since facies change relatively quickly in the lateral and vertical directions depending on their depositional environment (Li et al., 2012). To overcome this obstacle, several methods have been postulated to estimate the channel belt dimensions quantitatively (Bridge and Mackey, 1993; Bridge and Tye, 2000; Lorenz et al., 1985), as well as fluvial architecture and sandstone connectivity (Allen, 1979; Bridge and Mackey, 1993; Charvin et al., 2011; Hajek et al., 2010; Larue and Hovadik, 2006; Straub et al., 2009) from well log data.

The identification of fluvial architectural elements from log motifs is necessary for estimating channel belts. Log motif is used to identify different fluvial architectural elements. The channel belt dimensions are then estimated using empirical equations. Although these concepts provide valuable information on fluvial reservoir dimensions and their connectivity, they are not commonly used in reservoir characterization studies, even in places without seismic data.

Pattani basin hosts reservoirs of fluvial origin in different fields. Several studies have shown that the reservoirs here in Moragot are also fluvial in origin, but none of them have characterized them from the standpoint of where the sand was deposited in the fluvial system (Ahmad and Rowell, 2013; Hossain, 2018; Lambiase et al., 2016). There is a significant relationship between the depositional setting and reservoir properties. This study aims to identify where in the fluvial reach the different reservoir intervals are deposited. Then the characterization of these strata, which is also difficult as significant drilling depths (2500–4000 m), poor seismic resolution, and limited outcrop exposure, limit the ability to determine the

channel belt dimensions precisely. To overcome these impediments, this study aims to use empirical equations to estimate channel and channel belt dimensions, and then compare them with the channel and channel belt dimensions obtained from seismic geomorphology analysis, to determine the efficacy of the empirical equations. Correlating petrophysical properties of fluvial reservoirs in different zones with channel belt dimensions in the Moragot field is another goal of this research.

2. Study area

The study area is the Moragot field (Fig. 1). It is located in the southern Pattani Basin next to the Pailin field. A set of north-south oriented "Indosinian" fabrics along with a series of faults (Fig. 2a) developed during the collision of Indian and Eurasian plates are the main tectonic elements of the Pattani basin at a larger scale (Mountford and Morales Maqueda, 2019). The sedimentary sequences of post Oligocene time accumulated in the accommodation spaces created by post rifting activities (Crossley, 1990; Morley, 2013)

In the Pattani Basin, the Tertiary stratigraphic succession has been divided into five sequences based on both the litho- and seismic facies (Fig. 2b). They are divided on the basis of some well-defined regional markers (B, D, K, O). The sequences are named as sequence one in the bottom and sequence five in the top. In these sequences, the depositional environment ranges from fluvial to shallow marine. Tectonic activities and sea level changes influenced deposition in each sequence. The correlation of the sequences across the basin is performed based on lithostratigraphic correlation. A widely accepted depositional model of Pattani Basin was proposed by (Jardine, 1997).

Wells have been drilled from four platforms in this field. In total, there were 96 wells. Out of them, four wells (Fig. 1) from four platforms are selected to carry out this study. The selected wells contain the standard log suites (Table 1) and are sufficient to perform depositional environment analysis.

3. Methodology

3.1. Depositional environment analysis

Though the depositional environment of the reservoir sands is believed to be fluvial, it is important to further analyze this to understand the variations in dimensions of the channel belts. This has a significant impact on hydrocarbon production. For this reason, depositional environment analysis based on log motif has been performed.

3.2. Channel belt dimension analysis

3.2.1. Using empirical equations

Since 3D seismic data is sparse and their resolution decreases with depth several researchers have put forward some empirical equations to estimate channel belt dimensions (Bridge and Tye, 2000; Williams, 1986; Willis and Willis, 1989; Wu et al., 2015). Channel belt dimensions have been estimated from: 1) maximum bankfull flow Depth (CD) (m); 2) channel width (CW) (m); and 3) channel belt width (CBW) (m) in Fig. 3. Maximum bankfull flow depth represents the maximum depth of a river in flood and the flow depth at which most sandy bedforms are deposited (Bridge and Tye, 2000). The first step towards calculating channel belt dimensions is to identify the channel sand facies in the well logs. For making distinction between single and multi-storied channels, netto-gross cutoff values have been used. The sand-body thickness (ST) was determined from the logs after considering compaction effects.

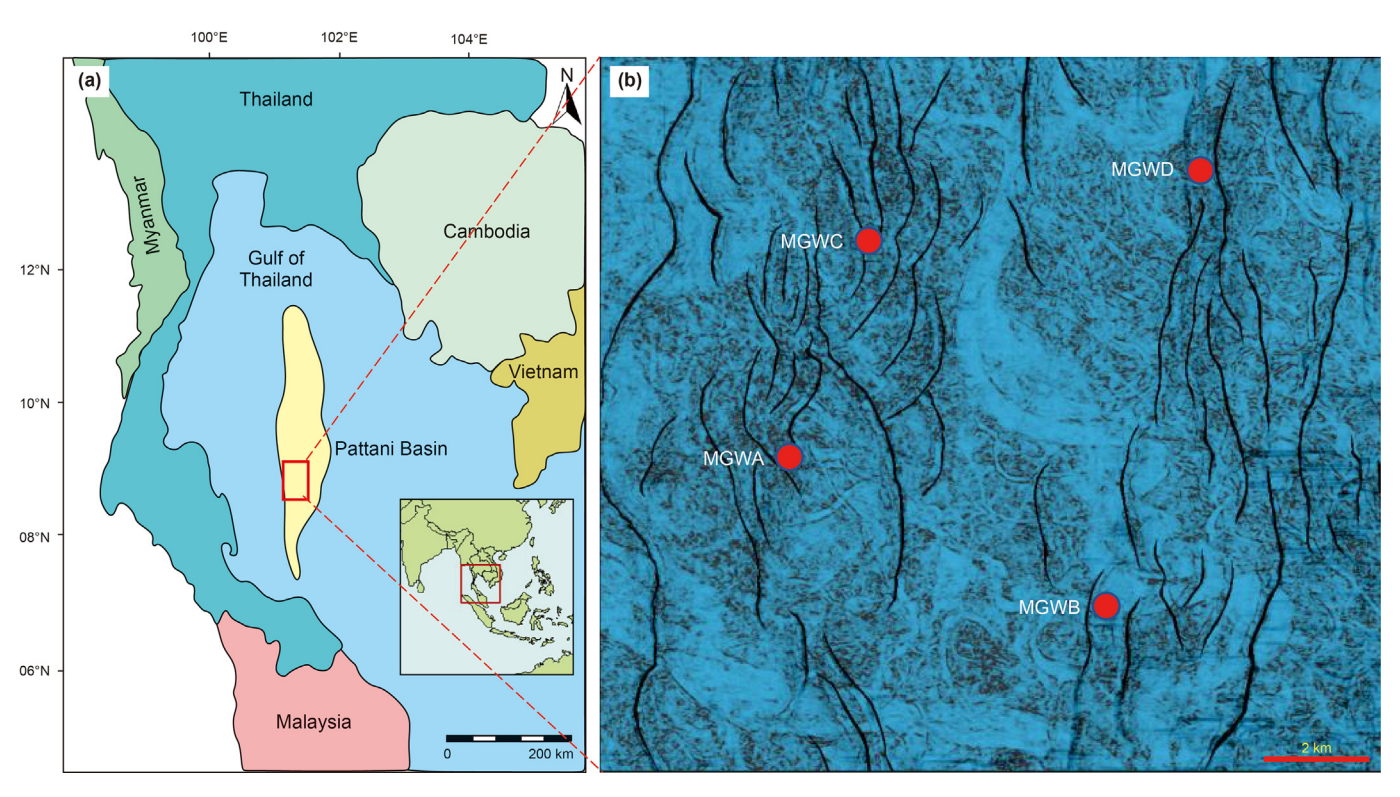


Fig. 1. Location map of the study area showing the location of Moragot field in Pattani Basin (a), and the location of the studied wells on a seismic attribute slice (b).

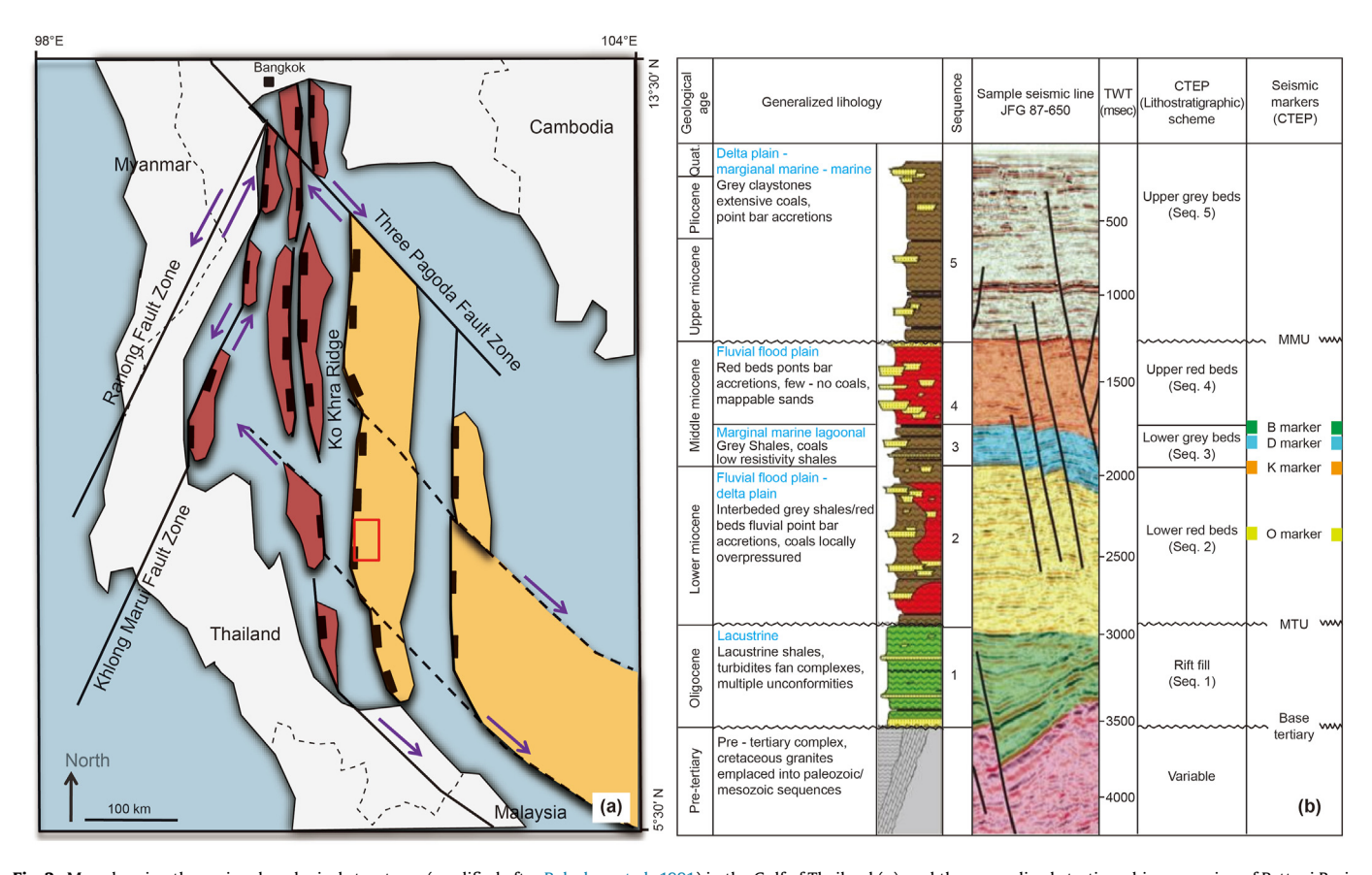


Fig. 2. Map showing the regional geological structures (modified after Polachan et al., 1991) in the Gulf of Thailand (a), and the generalized stratigraphic succession of Pattani Basin (by Jardine, 1997) with regional markers (b).

 Table 1

 Showing the studied wells with respective wireline logs.

Well Name	GR	DT	MSFL	ILD	RHOB	NPHI
MCMA						
MGWA	/	/	✓	/	✓	✓
MGWB	✓	✓	/	/	✓	/
MGWC	/	✓	1	1	/	/
MGWD	/	/	/	/	/	/

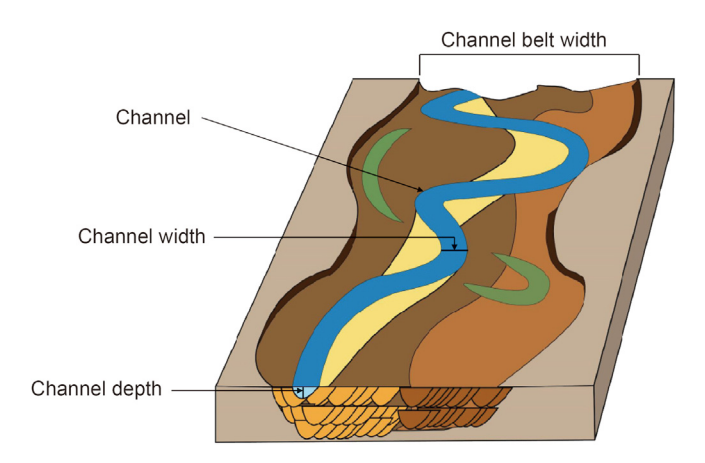


Fig. 3. Showing different parameters used for addressing channel belt dimension analysis.

The ST was chosen keeping in mind the effects if multistoried stacking.

The CD was determined by dividing the sand-body thickness by the CDST ratio (Fielding and Crane, 1987), as shown in Eq. (1)

Channel Depth
$$(CD) = \frac{\text{Sandbody Thickness}}{CDST}$$
 (1)

CDST values vary from 0.23 to 1 depending on the style of the fluvial system. Once the CD has been determined, the empirical relationship developed by (Leeder, 1973) from analyzing modern high sinuosity rivers (SN > 1.7) has been used for the determination of CW as shown in Eq. (2).

$$CW = 6.8 \times CD^{1.54}$$
 (2)

Finally, the channel belt width was determined using the relationship developed by (Lorenz et al., 1985) as shown in Eq. (3),

$$CBW = 7.44 \times CW^{1.01} \tag{3}$$

3.2.2. Seismic geomorphology analysis

Seismic geomorphology allows the identification of depositional features in the horizon and stratal slices (Reijenstein et al., 2011; Imran et al., 2020). For this first, the studied intervals are sliced through calculating several horizons in smaller time windows. After that, different seismic attributes are run to identify the depositional features and their dimensions.

3.3. Petrophysical analysis

Petrophysical analysis of the reservoirs has been carried out which has allowed us to evaluate them both from a quantitative and qualitative perspective. This has helped in specifying target reservoirs that can be more efficiently produced.

A number of approaches have been adopted in this study for the

estimation of the porosity of the reservoir units. Among them, the method for calculation of porosity from bulk density (Eq. (4)) has been noted to be the most representative, which is why it has been used as follows.

$$\varnothing_{\rm T} = \frac{\rho_{\rm ma} - \rho_{\rm b}}{\rho_{\rm ma} - \rho_{\rm f}} \tag{4}$$

where, \varnothing_T is the total porosity, ρ_{ma} is the matrix density, ρ_b is the bulk density and ρ_f is the fluid density.

Sonic porosity was used in places of bad holes found within the logs as follows,

$$\varnothing_{\mathrm{T}} = \frac{t - t_{\mathrm{ma}}}{t_{\mathrm{f}} - t_{\mathrm{ma}}} \tag{5}$$

where, $t_{\rm ma}$ is the travel time in matrix, t is the travel time in the formation and $t_{\rm f}$ is the travel time in the fluid.

The effective porosity is calculated by the following equation (Adams, 2005; Asquith, 1982; Worthington, 1988).

$$\varnothing_{e} = (\varnothing_{T}^{*} (1 - V_{sh}) \tag{6}$$

Permeability was determined based on Timur model (Timur, 1968) based on porosity and irreducible water saturation by using the following equation (Tiab and Donaldson, 2015).

$$K = 0.136* \frac{\emptyset^{4.4}}{S_{\text{wir}}^2} \tag{7}$$

where, K is the permeability of the formation in millidarcies (mD), \emptyset is the total porosity, S_{wir} is the Irreducible water saturation.

The irreducible water saturation has been calculated from water saturation (S_W) and effective porosity (\emptyset_e) using the equation $S_{Wir} = \frac{\emptyset^* S_W}{\emptyset_e}$.

The Indonesian model explained by (Pupon and Leveaux, 1971) has been observed to be a perfect method for the calculation of water saturation, in this case, keeping in mind the effects of frequent shale layers in the reservoir unit. The equation used is as follows

$$S_{W} = \left[\frac{V_{sh}^{1-(V_{sh} \times 0.5)}}{\left(\frac{R_{sh}}{R_{t}}\right)^{0.5}} + \left(\frac{R_{t}}{R_{o}}\right)^{0.5} \right]^{\frac{-2}{n}}$$
(8)

where $S_{\rm W}$ is the water saturation, $V_{\rm sh}$ the volume of shale, $R_{\rm sh}$ the deep resistivity reading in adjacent shale; $R_{\rm t}$ the true formation resistivity, $R_{\rm o} = \frac{\alpha \times R_{\rm w}}{O_{\rm c}^{\rm in}}$, $\alpha = 1$ and 0.62 for shale and sandstone, m = 2 and 2.15 for shale and sandstone, and n = 2.

Reservoirs in the Pattani Basin are mainly consists of moderately consolidated sands of Tertiary age (Ahmad and Rowell, 2013; Hossain, 2018). The values utilized for petrophysical analysis are taken from published literatures on this basin as well as in other parts of the world (Chow et al., 2005; Jardine, 1997; Kongwung and Ronghe, 2000; Lambiase et al., 2016; Mondol, 2015; Rider, 1996). The matrix and fluid density considered for petrophysical analysis are 2.65 g/cm³ and 1.03 g/cm³ respectively. Sonic travel time in the matrix and fluid are 54 μ s/ft and 189 μ s/ft. The tortuosity factor value for unconsolidated sand (a_{sand}) is 0.62 (Bernabé et al., 2010) and for shale (a_{shale}) is 1, is widely used in Archie's equation for water saturation calculation. The cementation factor (m) refers to the decreasing of size and number of pore spaces in a formation unit and is widely used by many authors for hydrocarbon and

reservoir evaluation (Jackson et al., 1978; Salem and Chilingarian, 1999; Verwer et al., 2011). Usually, the value of cementation factor ranges between 1.3 and 4.1 (Verwer et al., 2011), and it is affected by lithology, porosity, cementation, compaction and age (Richards, 1982). The cementation factor for unconsolidated sand ($m_{\rm sand}$) is 2.15 (Asquith, 1982) and for shale ($m_{\rm shale}$) is 2 are widely used in Archie's equation for water saturation calculation. Saturation exponent (n) value for a fully water saturated reservoir is 2 used in archie's water saturation equation. Standard values used for the parameters in the equations above have been listed in Table 2.

4. Results

4.1. Depositional environment analysis

The depositional environment of reservoir sands in the Pattani Basin is fluvial (Ahmad and Rowell, 2013; Hossain, 2018; Lundegard and Trevena, 1990). There have been several well log, seismic, and core data-based studies conducted in the Pattani Basin (Ahmad and Rowell, 2013; Kongwung and Ronghe, 2000; Lambiase et al., 2016; Zheng et al., 2003). Since fluvial systems show a wide variety and the fluvial system stretch for a long distance, it is essential to identify their type and where in the fluvial depositional spectrum these sediments are deposited. Based on their spatial position, there can be significant variation in the reservoir properties of fluvial deposits (Zhang et al., 2021). Several internal and external factors influence the dimensions and styles of fluvial systems. These influence result in fluvial deposits of different types. The deposits vary in size, texture, and composition. A well-developed meandering channel has very clean sand, whereas a channel influenced by marine environments has a lot more silt. Due to the variation in controls at different reaches, the fluvial stratigraphy in the upstream and downstream reaches differs significantly. This is why fluvial depositional models are not always useful. Separate treatment should be given to each fluvial system based on its reach, stacking pattern, and deposits. Hence, it is important to identify the different factors that affected paleochannel systems.

Most subsurface analyses are specific to certain fields. This is because data are rarely available outside the field boundary. This is the main challenge in interpreting depositional environments from subsurface data since they represent only a small part of depositional settings. Therefore, many interpretations of different scenarios are needed.

For the depositional environment analysis well log facies, their stacking pattern has been utilized. The depositional environment analysis was performed in the predefined three zones based on the regional marker horizons (B, D, K, and O) (Jardine, 1997). In total six (6) log facies are identified ranging from classic fining upward, blocky and crescent shape, etc. Each of them represents a different depositional process. Their interpretation is shown in Fig. 4. There are distinct differences between the deposits in the three zones.

Table 2Values used for calculation of petrophysical parameters.

Name of the Parameter	Symbol	Value
Matrix density Fluid density Travel time through the matrix Travel time through the fluid Tortuosity factor for sand Tortuosity factor for shale Constant Constant Saturation exponent	$ ho_{ m ma} ho_{ m f} ho_{ ho} ho_{ m f} ho_{ ho} ho_{ ho}_{ $	2.65 g/cm ³ 1.03 g/cm ³ 54 µs/ft 189 µs/ft 0.62 1 2.15 2

The fluvial reach in each zone was identified by the stacking pattern and the thickness of the different log facies.

4.1.1. Zone 1 (B to D)

This is the uppermost zone in the zone of interest. The wireline character of this part is represented by fining upward cycles (Fig. 5). Sands are thick in this interval, with an average sand thickness of 14 m. In general sand, the thickness is higher in the lower and middle parts of the interval. The fining upward succession is interpreted as the point bar deposits (Rider, 1996). These point bars formed due to the lateral migration of river channels. The basal sands indicate the channel deposits and the shales deposited in the floodplain. The net to gross in this interval is around 40%. All these observations are very suggestive of meandering river deposits. Hence the depositional environment of this zone can be interpreted as fluvial.

4.1.2. Zone 2 (K to D)

The wireline character of this part is represented by coarsening upward cycles. Sand thickness is considerably lower (Fig. 6) in this interval compared to zone 1 and zone 2. Hence this interval is shalier than the other zones. As interpreted by their low gammaray and low density, the abundance of coal deposits has been observed in this interval. The net to gross in this interval is less than 20%. It is assumed that the thin sand deposits in this interval are associated with narrow straight channels in a mud-dominated setting as the regional depositional environment, and they were fluvial dominated during this time with occasional marine transgression. Such straight channels with little or no lateral migration evidence suggest a low slope and low accommodation area similar to delta plain (Miall, 2002). It implies a deltaic progradation sequence (Rider, 1996) in a paralic setting. Hence, this zone is broadly interpreted as the marginal marine depositional environment. The interpretation is well supported by the widespread occurrence of coal, which has been characterized by low gamma values and extreme low density in logs.

4.1.3. Zone 3 (O to K)

This zone covers the lowermost part of the zone of interest. The wireline character shows the dominance of blocky and fining upward cycles (Fig. 7). Among the three zones, this interval shows the thickest sands. The average sand thickness is about 16 m. The fining upward successions are similar to the ones observed in zone 1. These are interpreted as channel sands and point bar deposits (Rider, 1996) associated with meandering river systems. The blocky pattern of thick sands indicates stacked channel deposits indicate fluvial deposits (Onyekuru et al., 2012) in their lower reach, where channels are confined within their channels with limited lateral movement. The thick sand deposits are most likely the stacked channel sands. Considering all these, this interval is interpreted as the fluvial-dominated depositional setting. Though both zone 1 and zone 3 show dominantly fluvial deposits, they show some differences in stacking patterns. It is inferred that zone 3 is more distal than zone 1.

4.2. Channel belt dimension analysis

4.2.1. Empirical equations

Fluvial channel deposits mainly occur in laterally confined, elongated belts, recording the limited capacity of the depositing channel to move laterally i.e., perpendicular to its palaeoflow direction. Depending on factors like sinuosity, discharge, and sediment supply the channel belt dimension varies significantly (Bridge, 1993). This is why estimating the channel belt widths in the subsurface is of paramount importance for exploration and field development. Modern 3D seismic data can be utilized to achieve

Log motif	Description	Interpretation
0 250 E	Low gamma ray value and an abrupt base at the bottom. Upward increasing GR creates a bell-shaped log motif.	The fining upward profile with an erosional base indicates that deposition was the product of bar migration in the channelized portion of a fluvial system. Deposits are attributed to single storey channel belts.
0 250 E	Consistent trend of low GR with sharp top and base edge gives a blocky/ cylindrical shape.	Coarse-grained sandy bedforms, multilateral and multistory amalgamated channel complexes; bedload filled channel (Hornung and Aigner, 1999).
0 250 E	Two vertically stacked low GR cylindrical shaped sequences separated by a thin layer of a high GR unit. Both the top and base are sharp.	Stacked units >10 m thick, lacking mudstone interbeds, represent amalgamated fluvial channel bars deposited in a single or multistorey channelbelt system as a result of vertical aggradation and lateral migration (Allen, Cabrera et al., 1983; Bridge and Tye, 2000; Miall, 2014; Heldreich, Redfern et al., 2017).
0 250 E	High gamma ray value and irregular pattern/ spikes of low GR values.	Fluvial flood plain deposit (Nazeer, Abbasi et al., 2016; Durkin, Boyd et al., 2017).
0 250 E 50	Gradual decrease in the GR value to the top shapes like a funnel, which is a cleaning up trend.	The funnel shapes represent coarsening- upward sequences that are interpreted as crevasse splay (Mondol, 2015; Nazeer, Abbasi et al., 2016).
0 250 E	Crescent or bow trend in the gamma ray log shows a cleaning-up trend overlain by a dirtying up trend without any sharp break.	Crescent log pattern is generally the result of waxing and waning elastic sedimentation rate.

Fig. 4. Summary of the log facies identified in all three zones. In total 6 log facies representing different depositional processes has been identified.

this information of channel parameters. However, when the depth increases seismic imaging gets very challenging as the vertical resolution decreases (Rafaelsen, 2006). Therefore, estimating channel belt dimensions from well log data is very useful. Throughout the years, geoscientists have studied fluvial channel systems (Bridge, 1993; Bridge and Tye, 2000; Durkin et al., 2017; Miall, 2002; Williams, 1986) and the nature of their dimensions around the world, and they have developed several empirical equations which can be used to estimate channel width and channel belt widths from sand body thickness obtained from well logs.

In this study channel belt widths have been estimated from sand-body thicknesses (ST) using a set of empirical equations. At

first, channel depth was estimated from the sand body thickness and CDST ratio using Eq. (1). Sand body thicknesses at different zones have been obtained from the well logs. A compaction factor of 10% was applied to the sand body thicknesses. For each zone, low, medium, and high values of sandbody thickness were considered. CDST ratio is a critical parameter to estimate as there is considerable uncertainty regarding the relationship between sandstone observed and bank-full depth of the formative channel. In many cases, channel depths may not have been as deep as preserved sandstone, due to the fact that channel systems can accrete vertically as well as laterally. It is also possible for the channel to be partially filled with mud-dominated channel abandonment facies. These lead to a wide range of variation in CDST ratios, from over 1: 1

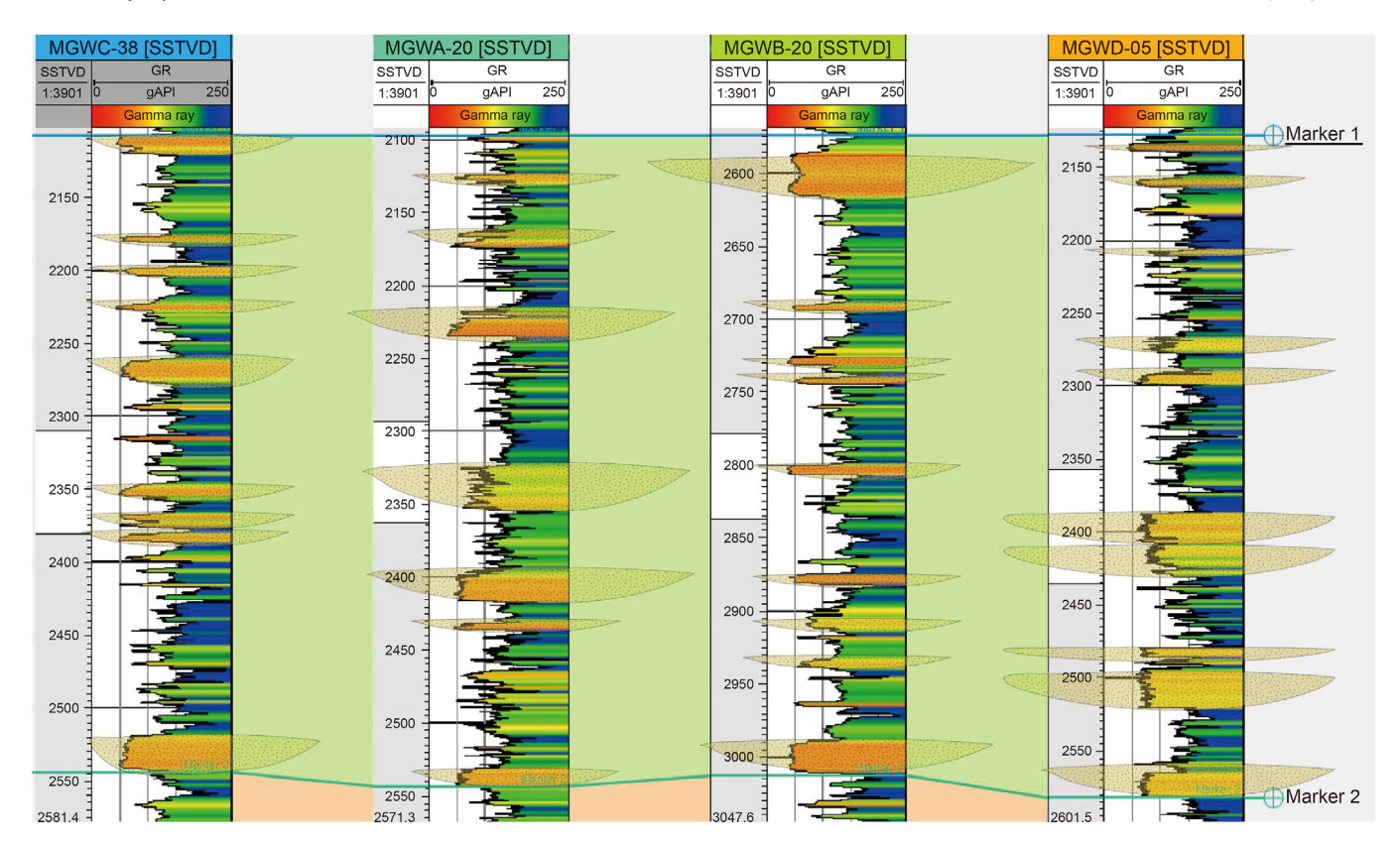


Fig. 5. Well correlation panel in zone 1 showing the average thickness of this zone in different wells and the thickness of the channel sands. The most abundant log motif is the classic cylindrical pattern with some blocky signatures.

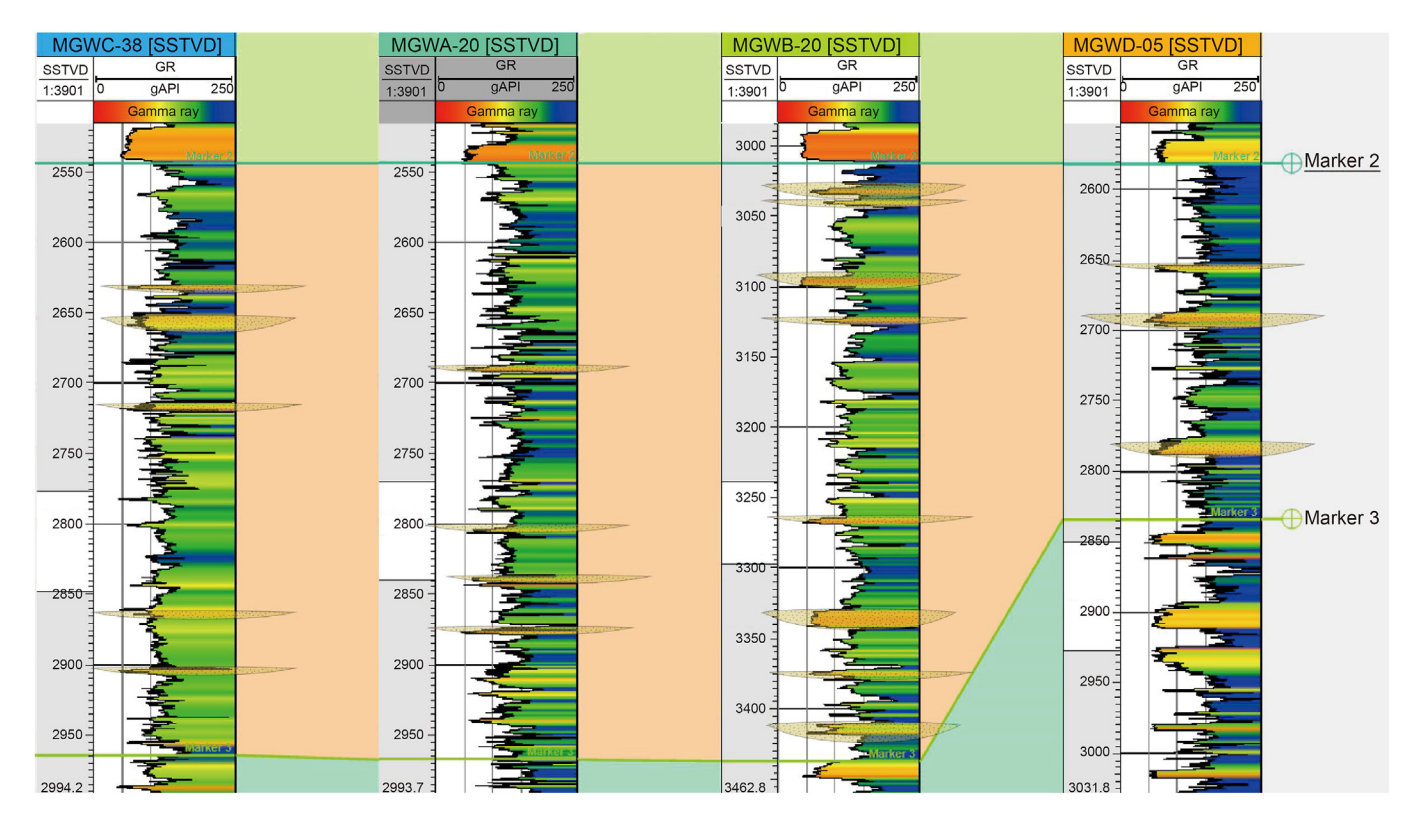


Fig. 6. Well correlation panel in zone 2 showing the average thickness of this zone in different wells and the thickness of the channel sands. The most abundant log motif is serrated pattern and funnel shaped cycles.

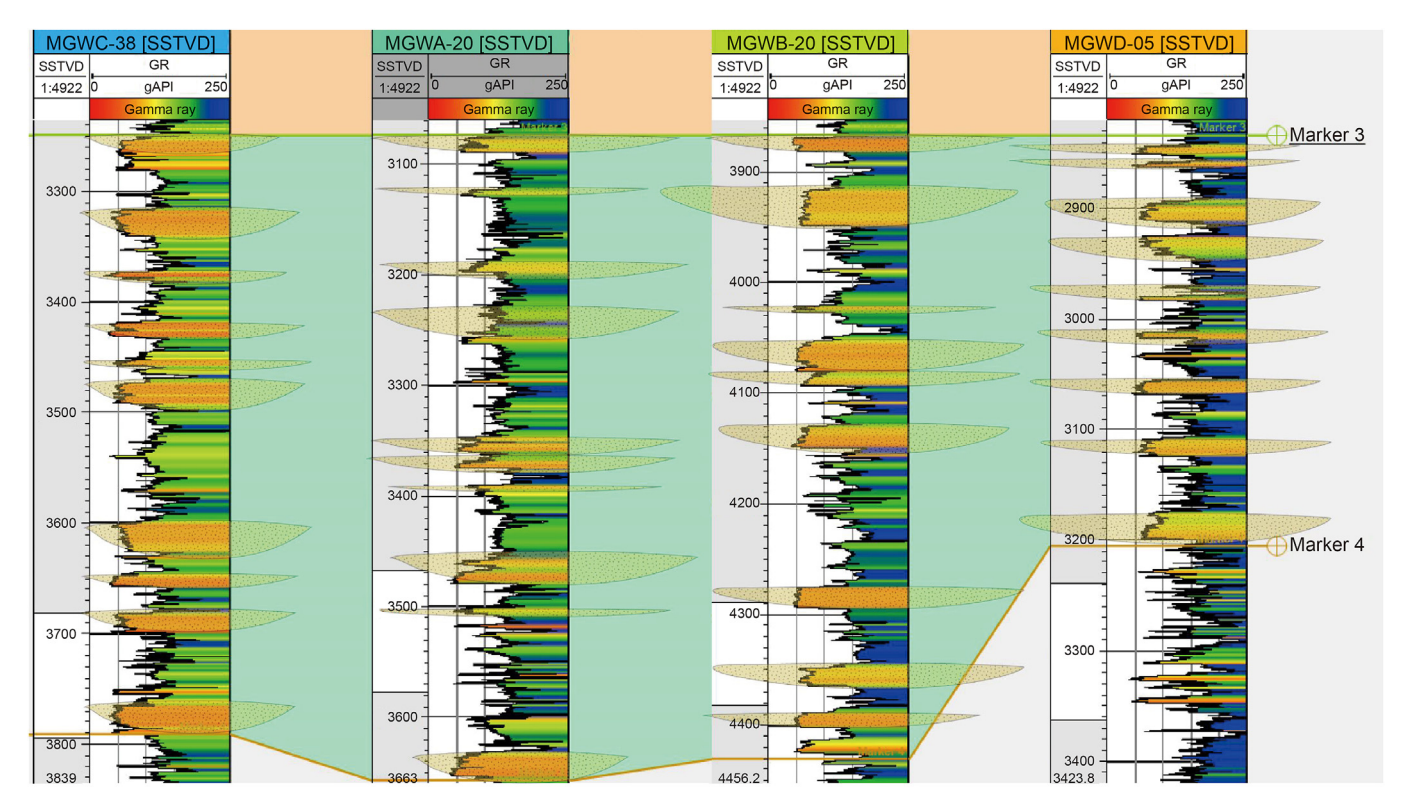


Fig. 7. Well correlation panel in zone 3 showing the average thickness of this zone in different wells and the thickness of the channel sands. The most abundant log motif is blocky and cylindrical pattern.

to 0.23: 1 (Fielding and Crane, 1987). Fielding and Crane (1987) collected channel depths and sand body thicknesses from a variety of fluvial system types and plotted them. They have an average CDST ratio of 0.775 across their data population, and the meandering system has one of the highest. A range of CDST 0.73–0.95 has been used in this study. The channel width was then calculated using Eq. (2) based on the estimated channel depth. Since the study interval is characterized by meandering channels with high sinuosity (Ahmad and Rowell, 2013; Hossain, 2018; Reijenstein et al., 2011), this equation is used. Finally, the channel belt dimension was calculated using Eq. (3).

By adopting interpretative techniques, the accuracy of paleochannel depth determination has been greatly affected.

The predicted channel belt widths as shown in Table 3 is quite analogous with the channel dimensions observed in the seismic time slices in Fig. 8. Analysis from 1D wireline log interpreted thickness has yielded morphological attributes of paleochannels which are acting as reservoir units.

4.2.2. Seismic geomorphological analysis

Seismic geomorphological analysis was performed to determine the pattern of fluvial systems and the dimensions of channels and channel belts (Fig. 8). To observe changes, 18 horizons have been calculated within the specified intervals. Then the RMS attribute was calculated for all horizons within a 20 ms interval. The RMS can clearly identify fluvial systems within zone 1 as shown in Fig. 8b, but as the depth increases, imaging becomes more challenging. The sporadic distribution of high amplitude is seen in most of the horizon slices in zone 2 as shown in Fig. 8c. This is mainly because of the widespread distribution of coals. Zone 3 represents a well-developed fluvial system. Channel patterns are not always evident in all slices because their thickness is less than the tuning thickness (Fig. 8d). In zones 1 and 3, the channels have similar

dimensions, whereas zone 2 has poorly developed channels.

4.3. Well log petrophysical analysis

The petrophysical study of three fluvial reservoir units revealed important information on their reservoir characteristic and petrophysical parameters. This provided the basis to categorize and predict reservoir behaviors and hydrocarbon production potentiality.

Petrophysical parameters have been estimated using standardized formulas and the values of the constants used for the calculations have been used based on regional lithological characteristics shown in Table 3. The three reservoir zones form three distinct clusters as shown in the neutron density cross-plot (Fig. 9a). The depositional environment interpretation clearly indicates a more fluvial dominance with zone 1 and zone 3 showing greater similarity, while zone 2 represents a more marginal marine-influenced fluvial setting. The cross-plot compares the properties and identifies distinct facies present within the three zones. The neutron values in zone 1 and zone 3 clusters in Fig. 9a are similar but the densities are very different. Compaction due to overburden pressure resulted in density variation. Being the oldest unit among the three, zone 3 was subjected to a greater depth than zone 1, causing its intergranular spaces to be significantly affected.

A facies characterization has been made using the neutron density plot in Fig. 9b. It has been found in the plot that the coal layers frequently observed in the logs are clustered with a low density and a high neutron value, which is attributed to their capacity to store significant amounts of water. The shale units were characterized by high density and neutron values, along with high gamma rays. The gas sand cluster represents low density and low neutron values making them easier to identify, and lastly the wet sand cluster is characterized by its high-density values and

Table 3 Fluvial channel and channel belt dimensions estimated using empirical equations.

Zone	Sand body thickness, m	CDST	Channel depth	Channel width	Channel belt width
Zone-1	4	0.73	5.48	93.36	726.84
		0.87	4.60	71.26	553.25
		0.95	4.21	62.23	482.50
	9	0.73	12.33	325.48	2565.80
		0.87	10.34	248.42	1953.02
		0.95	9.47	216.94	1703.27
	12.5	0.73	17.12	539.80	4276.89
		0.87	14.37	411.99	3255.46
		0.95	13.16	359.80	2839.16
Zone-2	2	0.73	2.74	32.11	247.30
		0.87	2.30	24.50	188.24
		0.95	2.11	21.40	164.16
	3.5	0.73	4.79	76.01	590.52
		0.87	4.02	58.01	449.49
		0.95	3.68	50.66	392.01
	6.5	0.73	8.90	197.19	1546.68
		0.87	7.47	150.50	1177.29
		0.95	6.84	131.43	1026.74
Zone-3	4.5	0.73	6.16	111.93	872.97
		0.87	5.17	85.43	664.49
		0.95	4.74	74.60	579.51
	8.5	0.73	11.64	298.06	2347.54
		0.87	9.77	227.49	1786.89
		0.95	8.95	198.66	1558.38
	13	0.73	17.81	573.41	4545.92
		0.87	14.94	437.65	3460.24
		0.95	13.68	382.20	3017.75

relatively higher neutron values compared to the gas zone. The interpretations are further supported by the gamma ray values. Coloring the distinct clusters of facies identified. Shale has been characterized by gamma values greater than 130, coal has gamma values 80–120 and the sand units less than 80. Integrating the data represented by the two plots it is quite correlative with the depositional model that has been suggested earlier. The dominant hydrocarbon bearing reservoir units in zone 1 and zone 3 are fluvial reservoirs, whereas zone 2 has lesser hydrocarbons. Zone 2 is characterized by a high coal content and a high proportion of shale, indicating marginal marine influence.

4.3.1. Porosity

The porosity of a reservoir is one of the most important petrophysical properties. It is a measure of the total amount of void space in a rock. We have estimated the porosity in two main ways, from density log using Eq. (4) and for cases where bad holes were encountered, density porosity was replaced by sonic porosity, using Eq. (5). The dominant constituent mineral for the sandstone reservoirs is dominantly quartz, keeping this in mind the value considered for matrix density was, $\rho_{\rm ma}=2.65\,{\rm g/cm^3}$. The wells were drilled with saline water-based mud, which is why the fluid density was considered as $\rho_{\rm f}=1.06\,{\rm g/cm^3}$. The travel time through the matrix was taken to be $t_{\rm ma}=54\,\mu{\rm s/ft}$ and through the fluid $t_{\rm f}=189\,\mu{\rm s/ft}$.

As observed in Fig. 10 around 32% of the porosity is observed in zone 1 with a mean value of about 26%. Zone 2 has the lowest porosity values with mean values of around 15%, and zone 3 has the intermediate values with mean values of around 20%. There is a negatively skewed distribution of porosity in zone 1, indicating high end porosity values are the dominant feature. Zone 2 displays a more symmetrical normal distribution, while zone 3 exhibits a bimodal distribution.

4.3.2. Permeability

Production of hydrocarbons depends largely on reservoir

permeability. There is a correlation between permeability and the nature and rate of connectivity between the pores present within the reservoir (Bernabé et al., 2010; Cai et al., 2019). The permeability within the reservoir is mainly dependent on the grain size, grain orientation, and their distribution. In addition to this, permeability within reservoirs is also influenced by diagenetic effects and the nature of shale distribution (Opuwari et al., 2021; Usman et al., 2020). As observed in Fig. 11, the best permeability is observed in zone 1, while lowest values are observed in zone 2 and a bimodal distribution with average values is observed for zone 3.

4.3.3. Water saturation

Water saturation is the percentage of water present within the pore spaces of a reservoir. There is a direct correlation between the amount of water saturation and porosity. The saturation values in the reservoir have been compared for reservoirs (Fig. 12a) and pay sand (Fig. 12b). Pay sand thickness was calculated by applying a 60% water saturation cut off. Zone 1 has the least amount of water saturation, while zone 2 has the most water saturation, and zone 3 has an intermediate amount of water saturation. In zone 2, water saturation is highest due to higher shale percentage.

4.3.4. Shale distribution

The nature of shale distribution within the reservoir is mostly laminated and dispersed in nature, as revealed from the Neutron Porosity versus Density Porosity cross-plot (Fig. 13). The gas effect is evident in rising values for the zone 1 and zone 3 because of having higher saturation of hydrocarbon in them, while the upward shift of zone 2 is suspected to be caused by the presence of organic matter within the high amounts of shale which is present in this zone.

By analyzing the porosity of the sand units, the amount of diagenetic effect on the reservoir rocks was evaluated. In the sonic and neutron porosity cross plot in Fig. 13, the data distribution of the data points of each zone reveals the porosity types present. In zones 1 and 2, the dominant porosity type has been interpreted as intergranular, whereas in zone 3, secondary porosity has been

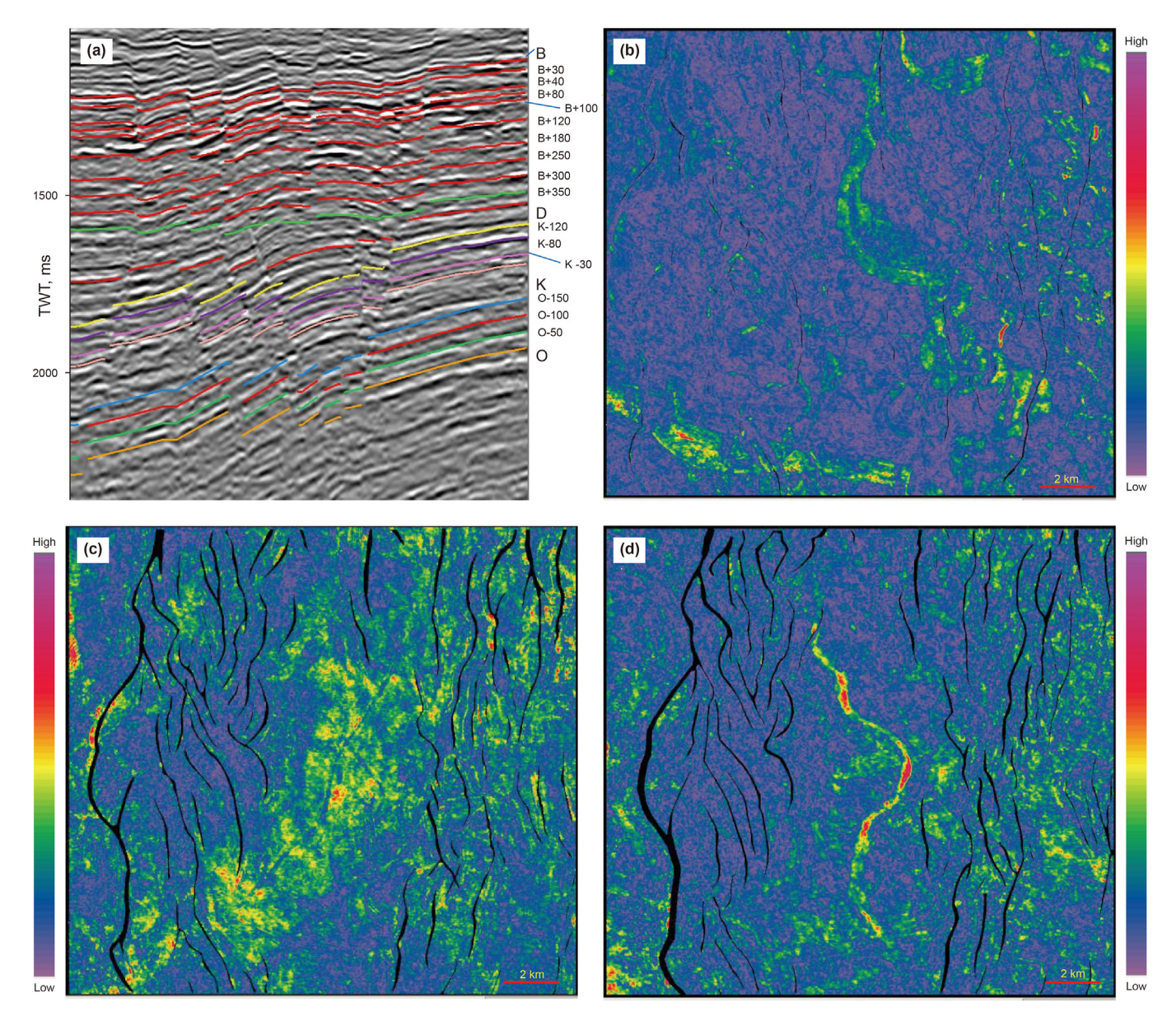


Fig. 8. The main horizons and the calculated horizons (a), representative stratal slice showing fluvial features in zone 1 (b), zone 2 (c), and zone 3 (d). Well developed fluvial features are clearly seen in zone 1 and 3. High amplitudes in zone 2 are related to the presence of extensive coals.

observed, which has been attributed to dissolution or any other secondary porosity enhancement process.

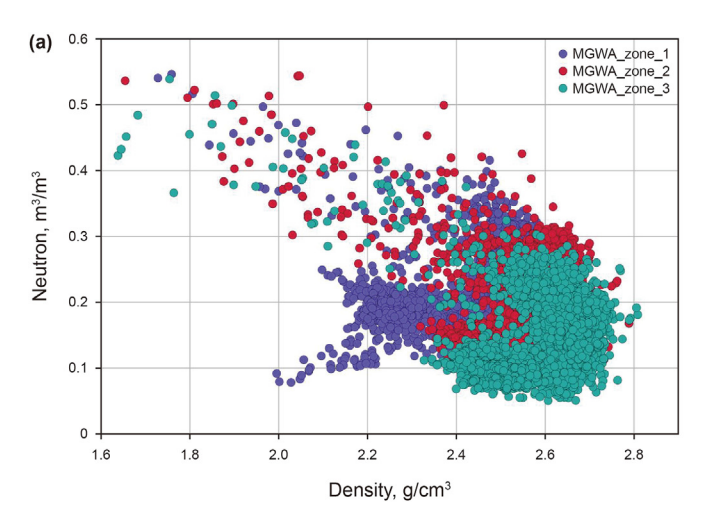
5. Discussion

After careful observation and thorough interpretation of the log motifs, 6 different log facies have been identified. Based on the evidences from well log analysis, it is interpreted that the reservoirs are fluvial dominated; however, their deposition has taken place at various fluvial reaches (Fig. 15). Some deposited in the upper and middle reaches of the fluvial system, whereas others deposited in the lower reaches of fluvial system grading into the marginal marine setting. Based on the evidence, it is interpreted that the depositional systems evolved in the following order. At first, the lower reservoirs deposited in a fluvial dominated depositional setting, then this area experienced a sea-level rise. During this zone, middle reservoirs deposited in the marginal marine setting (Fig. 16). The widespread occurrence of coal and thin reservoirs in

this interval are suggestive of the marginal marine condition. After that, sea level retreated, and the upper reservoir deposited by meandering rivers in their upstream reaches.

The most effective way of modelling fluvial reservoirs is to determine the paleoflow directions and identify the channel belt dimensions like thickness, width and belt width of the channels. In this study, the various facies related to fluvial channels have been identified, and bankfull channel depth has been determined after careful interpretation from the logs. Finally, the use of a suitable empirical equations has given the channel width and channel belt width which are important for understanding the reservoir extent. As observed in the seismic horizon slices in Fig. 8, the channels identified have dimensions quite identical to the values predicted by the empirical equations. It is quite noticeable that the channel patterns observed in the stratal slices representing horizons in the three zones studied in this research, are quite distinct from each other.

Fluvial systems in the stratal slice of zone 1 are quite prominent



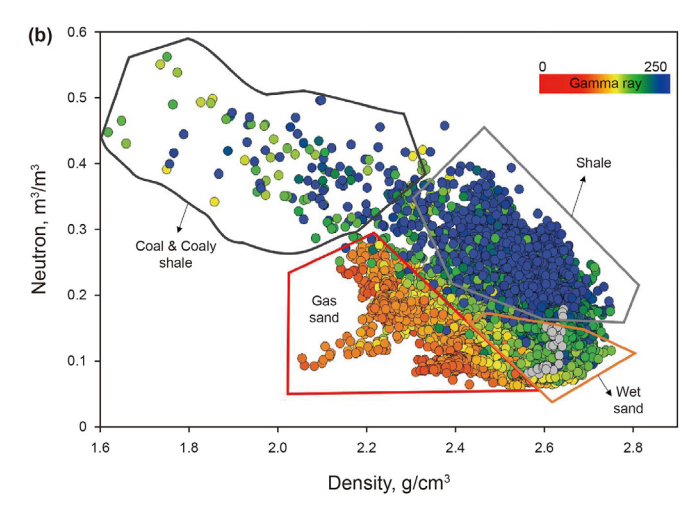


Fig. 9. Density-neutron crossplot representing the clusters of three zones (a) and showing different facies color coded by gamma ray (b).

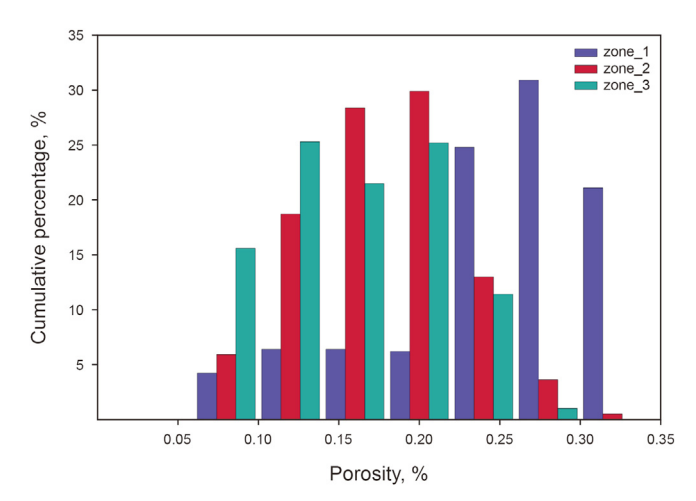


Fig. 10. Histogram of porosity distribution in the three zones shows zone 1 has the highest porosity and zone 2 has the least.

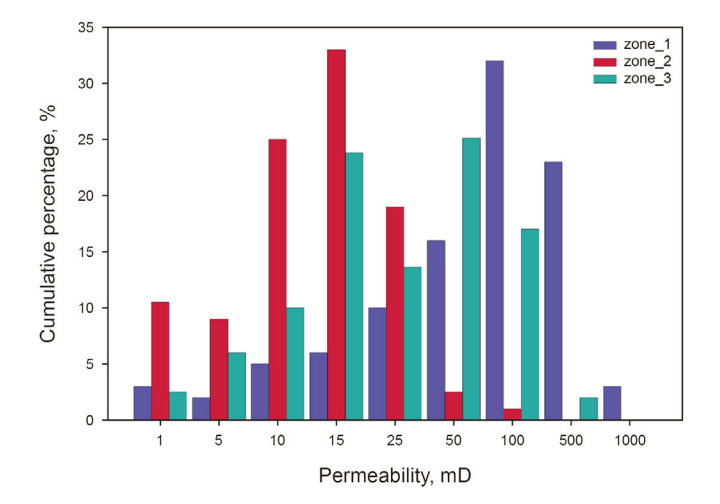


Fig. 11. Histogram of permeability distribution in the three zones shows zone 1 has the highest permeability and zone 2 has the least.

and recognizable because of the shallower depth, whereas the channel pattern observed in the stratal slice of zone 2 is quite obscure because of lower sand thickness and presence of coals. Though well logs show very well-developed fluvial sequences in zone 3, stratal slices could not image the fluvial systems properly. This is mainly because sand thickness at this interval is considerably lower than the tuning thickness. In some slices of zone 3, some parts of channels are visible and channel parameters were estimated making inferences based on seismic amplitudes.

This is case of all seismic data. They lose resolution as the depth increases. A solution to all these drawbacks of seismic imaging could be the use of empirical equations for characterizing fluvial reservoir architecture has been portrayed with suitable justification in this study. Table 4 shows a comparison made between estimated channel dimensions and dimensions obtained from seismic time slices, which clearly indicates that channel belt dimensions obtained from seismic amplitudes are in similar range with the one that obtained from empirical equations.

Petrophysical analysis was performed to identify the best reservoirs and relationship between the channel belt dimensions and the petrophysical parameters. The porosity values comply admirably with the interpretations made above. The three studied zones give three distinct clusters when plotted in gamma versus density porosity cross-plot. The gamma ray signatures for both zone 1 and zone 3 observed in Fig. 17 are quite identical while on the contrary, the porosity values differ significantly. On the other hand, zone 2 is characterized by high gamma values with low amounts of porosity which is due to the presence of excess amounts of shale within the reservoir.

Several factors combined together makes the porosity values of zone 1 the highest among the three studied zones. Zone 1 is comprised of sand-bodies deposited by well-developed meander belts as observed in the seismic time slices in Fig. 8. Furthermore, this zone occurs at the shallowest depth making the effects of compaction minimum. The pore spaces within the grains are well preserved and they are mostly intergranular, i.e., the effects of diagenesis are not yet significant.

It is observed in the neutron-porosity versus sonic-porosity cross-plot of Fig. 14 that the data points from zone 1 are dominantly indicative of primary porosity. This is why a negatively skewed unimodal porosity distribution in observed in Fig. 10.

The nature of grain to grain contact has also been evaluated using rock physics as a tool. In Fig. 18, it is observed that the three zones when plotted in the P-velocity vs porosity plane after suitable adjustment, indicated soft nature within the rocks. Comparatively within the three zones, the position of zone 1 indicates most soft

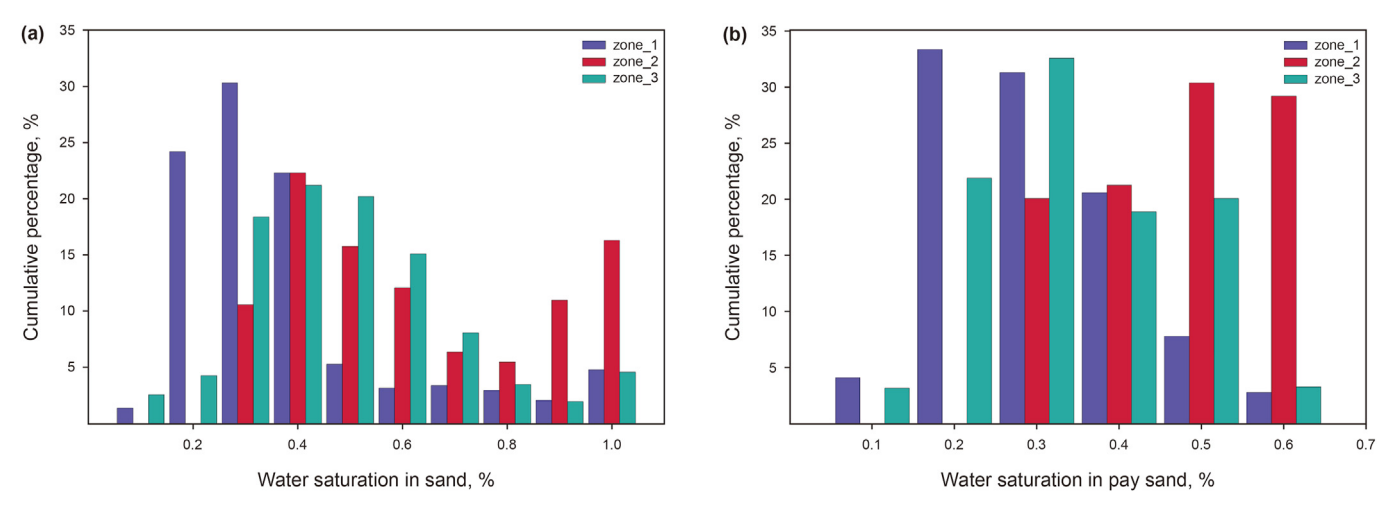


Fig. 12. Histogram of water saturation distribution in sand (a) and in pay sand (b) in three zones.

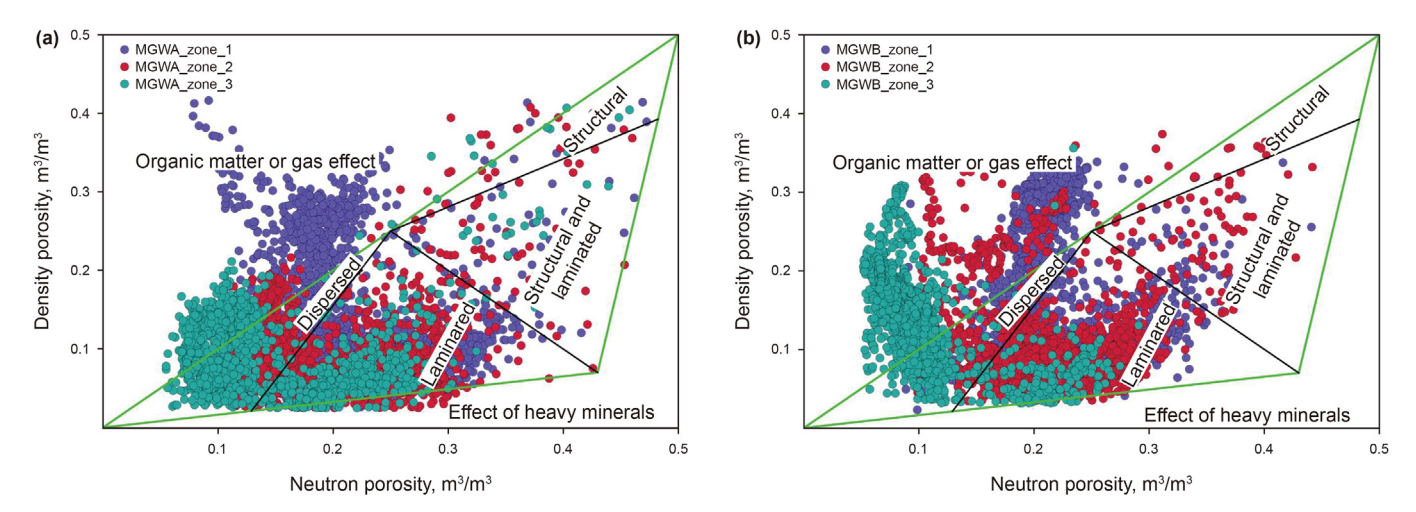


Fig. 13. Density porosity-Neutron porosity crossplot of MGWA (a) and MGWB (b) wells showing the shale distribution pattern in three zones.

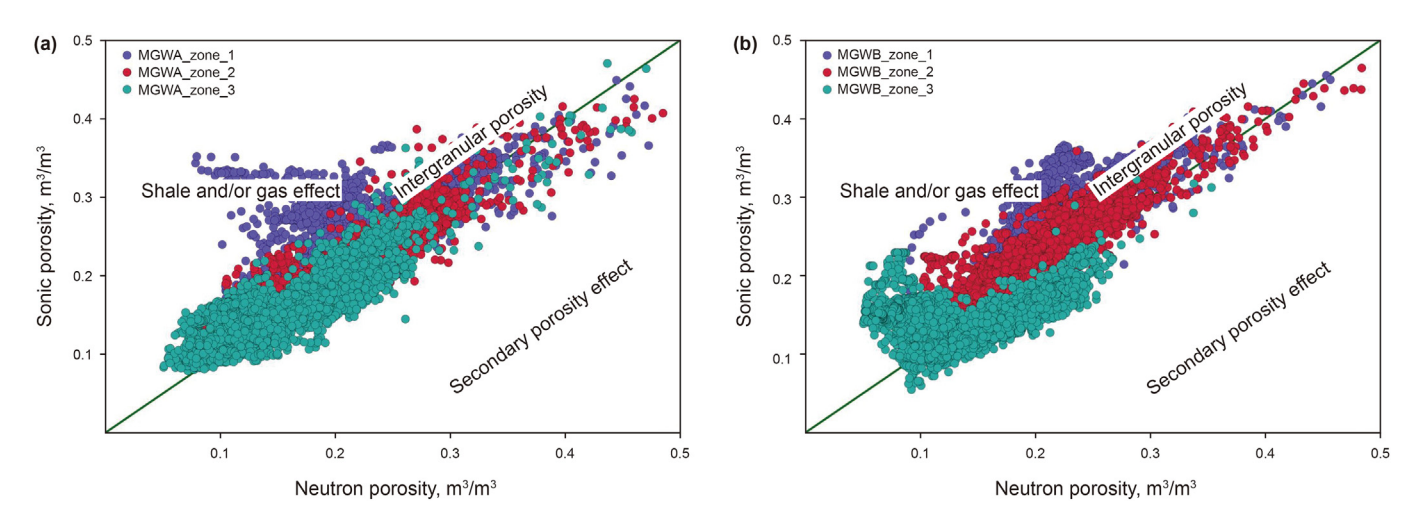


Fig. 14. Sonic Porosity-Neutron porosity crossplot of MGWA (a) and MGWB (b) wells showing the porosity type in all three zones.

nature, which also explains the reason behind higher porosity values in this zone. As observed in Fig. 11, the permeability values

for zone 1 are also the best among the three. Higher amounts of sand with good porosity helped in maintaining good permeability

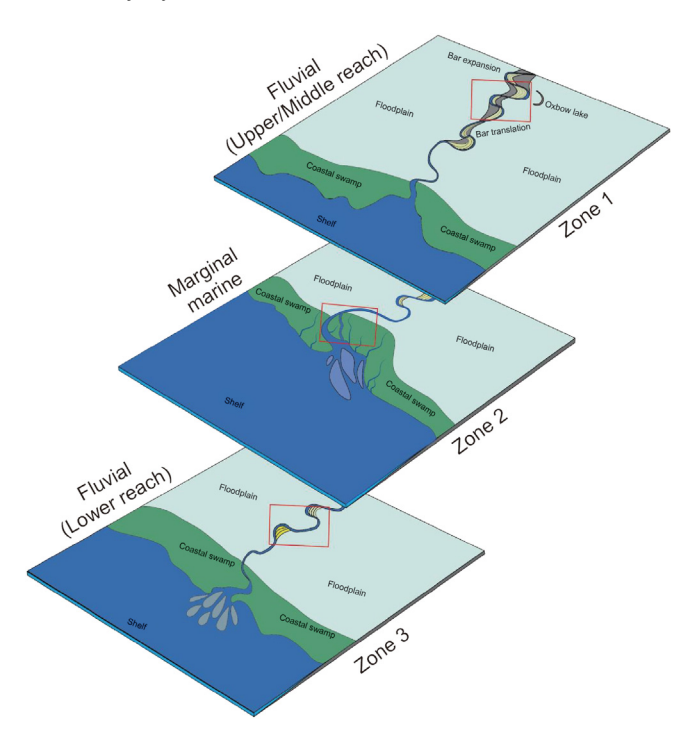


Fig. 15. Evolution of the depositional system through time. Depositional environments evolved from fluvial to marginal marine and finally back to fluvial again. Red boxes indicate the depositional setting of each zone.

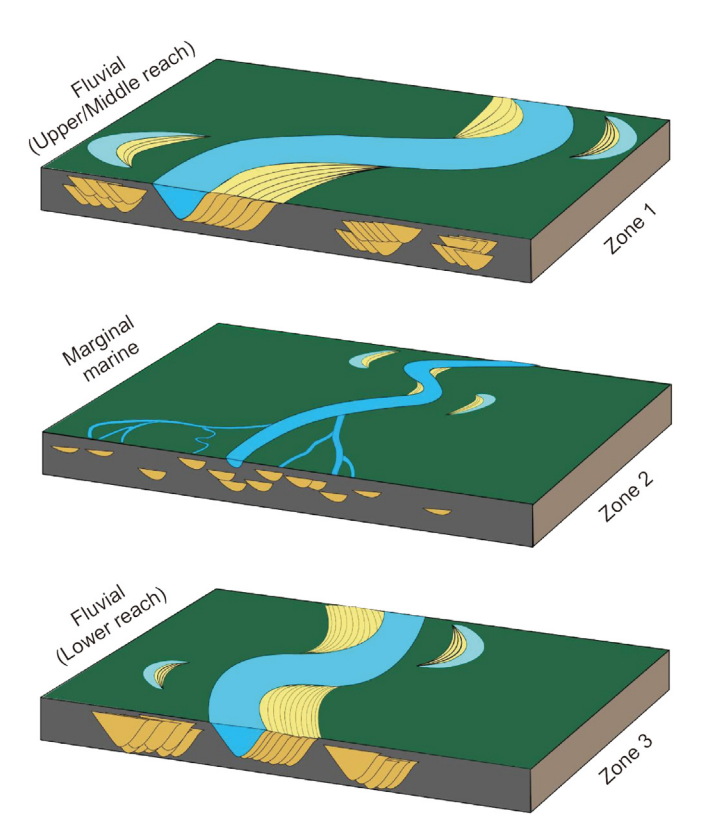


Fig. 16. Conceptual model showing deposition at different fluvial reaches. Meander belts are broader and more sinuous in zone 1 than zone 3 as indicated the blockier log motif in zone 3. Due to the proximity towards the coast main channel is branched into smaller channels in zone 2.

within the zone (Abuamarah et al., 2019; Magoba and Opuwari,

2020). Moreover, as observed in the neutron porosity versus density porosity cross plot of Fig. 13, the data points of zone 1 are clustered more towards the laminated zone, which indicates laminated nature of shale distribution within the reservoir sands. This type of reservoirs limits the vertical movement of fluids, but allows uninterrupted lateral flow within the rock. The water saturation within sand units as a whole for this zone is very low as seen in Fig. 12. The water saturation within the pay sands measured separately (Fig. 12b) also gives consistent results making it a suitable target for successful hydrocarbon production.

Zone 2 accounts for a more shale dominated reservoir unit. The seismic time slices for this interval shows sporadic distribution of amplitudes. Some narrow channels have been identified in some of the slices of this zone. The excess amounts of shale within this zone are interpreted to be the result of marine transgression. This is why the net to gross within this interval is also low. The porosity values within this zone as shown in Fig. 10 are comparatively low because of the dirty nature of the sand units. As observed in Fig. 13 the shale distribution within the reservoir units of this zone is more dominantly laminated with some amounts of dispersed shale, which has significantly influenced connectivity within the pores. The effects of dominant impermeable shale units observed within zone 2 combined with the nature of shale distribution within the reservoir sands, the permeability values observed in Fig. 11 for this zone are quite low. The property of shale to retain water within its structure has been clearly reflected in the water saturation values displayed in Fig. 12. The water saturation within this zone shows a bimodal distribution which is due to the presence of both reservoir sands and shale dominated non-reservoir rocks. The shale units account for abnormally high-water saturation values while the pay sands within the reservoir is characterized by lower amounts of saturation. But compared to other zones, the saturation within the pay sand is also quite high, overall making this zone an unsuitable target for exploration.

As evident from Fig. 17, zone 3 has similar gamma values to that of zone 1 because of having been deposited in similar conditions thus having similar net to gross percentages. The main difference observed is in the porosity values. The porosity has been significantly diminished due to the effect of compaction. Greater burial depths have not only reduced the porosity but have also induced diagenetic effects. In Fig. 10, a bimodal porosity distribution pattern is observed which is speculated to be the effect of diagenesis. In support to this data clusters of zone 3 in Fig. 14, it indicates both primary and secondary porosity. The present state of the rocks has been achieved after a series of diagenetic events, initially the primary porosity within the rocks had been filled in by cement and then these cemented spaces had been freed up by the process of dissolution which are now acting as secondary pores. The grain to grain nature of contact between the grains inferred using rock physics templates are also observed to be more stiff in nature among the three zones in Fig. 18. The nature of shale distribution within the reservoir are also both laminar and dispersed as shown in Fig. 13. A significant difference observed in this zone when compared to zone 1, the data points form prominent clusters in both the laminated and dispersed territory. The effects of secondary porosity are also reflected in the permeability values displayed in Fig. 11, where a bimodal distribution is found for this zone.

Fluid flow within the rocks is not of uniform nature because of presence of cemented spaces and compacted pores. The reduced porosity within this zone has also caused the pore throats diameters to reduce in size which has triggered the capacity of the rocks to store more water (Fig. 12) within the pore spaces due to capillary action. The three reservoir units focused in this study are all results of fluvial deposits and as reflected from their petrophysical statistics, it is quite perspicuous that the reservoir quality

Table 4Comparison of channel and channel belt dimension obtained from empirical equation and seismic geomorphology analysis

Zone	Well log empirical equation	ns	Seismic time slices	
	Channel width, m	Channel belt width, m	Channel width, m	Channel belt width, m
Zone 1	62-539	482-4276	93-484	474–4168
Zone 2	21-197	164-1547	36-234	206-1823
Zone 3	75–574	664-4546	127-530	825-4500

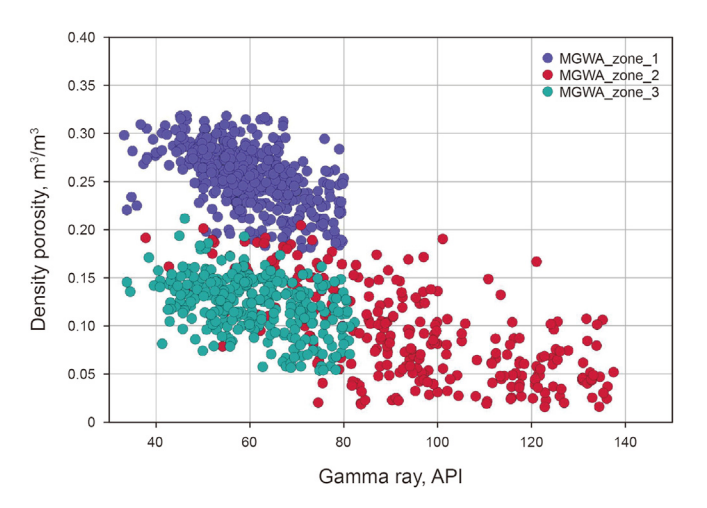


Fig. 17. Crossplot between density porosity and gamma ray showing three distinct cluster of porosity of three zones.

of the sandstone deposits is overall quite good.

Comparing the three reservoir units with each other they show some generic differences in stacking pattern, directly related to their depositional environment which are quite crucial from the reservoir perspective. Detailed analysis of reservoir architecture giving significant insight into the subsurface extent and morphological nature of the reservoir integrated with the petrophysical evaluation leads to the conclusion that zone 1 is the best prospect among the three reservoir units studied followed by zone 3 and lastly zone 2.

6. Conclusions

The log motif analysis has proven to be a very helpful tool in

determining the depositional environments of the Moragot field's study interval. To identify the depositional system, the study interval is divided into three zones based on the regional marker horizons. There are two primary depositional settings - fluvial and marginal marine. Overall, the depositional system is fluvial dominated. The lower part of the study interval, i.e., zone 3, deposited in fluvial environments, and then in zone 2, the depositional environment changed into a marginal coastal environment, probably due to sea level rise. The upper part of zone 1, deposited in a fluvial environment, implying a retreat of the sea level. Log motif in zone 1 is well developed finning upward sequences, suggesting proximal part of meandering fluvial system, whereas in zone 3 fining upward sequences are not well developed. These apparent blocky nature of sands in zone 3 in an overall fining upward sequence suggests distal reach of meandering fluvial system. Sand thickness is greater in zones 1 and 3 than anywhere else. The reservoirs in zone 2 are thin. A depositional model has been developed to explain the transition of the fluvial environments from one zone to another.

Empirical equations and seismic geomorphological analysis are used to calculate the dimensions of the fluvial channel belt. It is found that the channel dimensions obtained from empirical equations are of similar magnitude to the ones seen in seismic horizon and stratal slices in different intervals. The findings were very similar despite different means of estimating. Hence these empirical equations can be used to estimate channel belt dimensions in places where there is no seismic data. Detailed petrophysical evaluations have indicated that zone 1 has the best quality reservoirs. Zone 1 and zone 3 are lithologically similar, but because of the diagenetic effect, zone 3 has poorer reservoir properties than zone 1. The reservoirs in zone 2 are of the poorest quality due to their depositional setting in marginal marine environment.

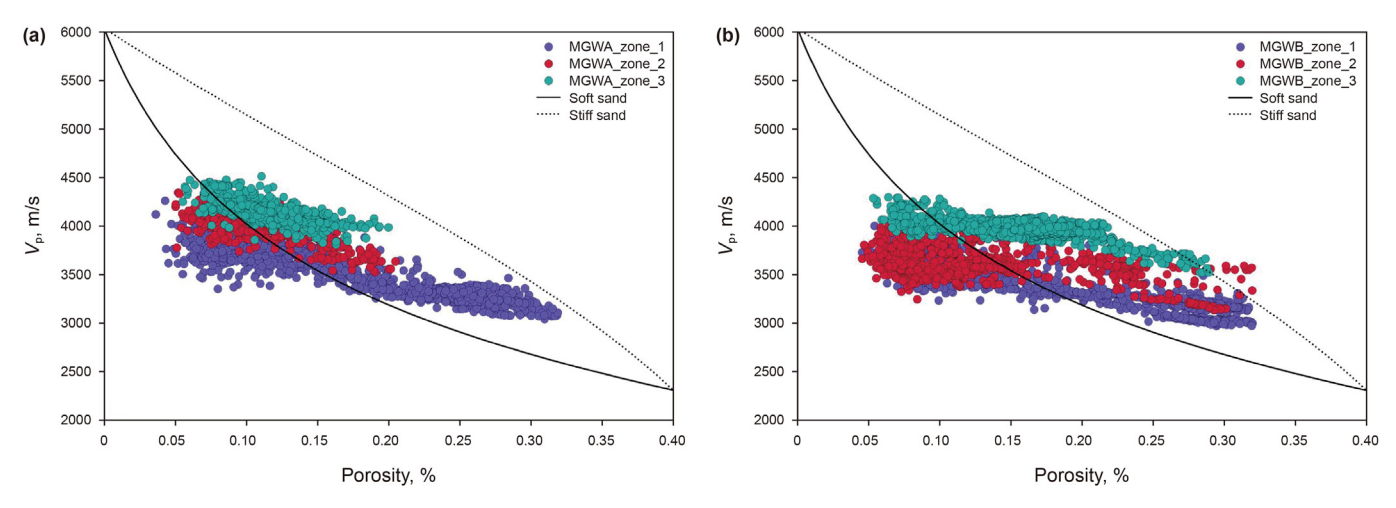


Fig. 18. Crossplot between P-velocity and porosity showing the nature of the reservoir sands of three zones.

Authors' contributions

Conceptualization: [Shakhawat Hossain]; Methodology: [Shakhawat Hossain, Tahmidur Rahman Junayed]; Formal analysis and investigation: [Shakhawat Hossain, Tahmidur Rahman Junayed, Naymur Rahman]; Writing-original draft preparation: [Shakhawat Hossain, Tahmidur Rahman Junayed]; Writing - review and editing: [Shakhawat Hossain, Tahmidur Rahman Junayed, Naymur Rahman]

Availability of data and material

The datasets generated during and/or analyzed during the current study are available from the corresponding author on reasonable request.

Declaration of competing interest

The authors have no conflicts of interest to declare that are relevant to the content of this article.

Acknowledgment

The authors would like to convey his gratitude to Chevron Thailand and Chulalongkorn University for providing data and logistics required to carry out this research work.

References

- Abuamarah, B.A., Nabawy, B.S., Shehata, A.M., Kassem, O.M., Ghrefat, H., 2019. Integrated geological and petrophysical characterization of oligocene deep marine unconventional poor to tight sandstone gas reservoir. Mar. Petrol. Geol. 109, 868–885. https://doi.org/10.1016/j.marpetgeo.2019.06.037.
- Adams, S., 2005. Quantifying petrophysical uncertainties. All Days. https://doi.org/ 10.2118/93125-ms
- Ahmad, M.N., Rowell, P., 2013. Mapping of fluvial sand systems using rock physics analysis and simultaneous inversion for density: case study from the Gulf of Thailand. First Break 31 (5). https://doi.org/10.3997/1365-2397.2013012.
- Allen, J.R.L., 1979. Studies in fluviatile sedimentation: an elementary geometrical model for the connectedness of avulsion-related channel sand bodies. Sediment. Geol. 24 (3-4), 253-267. https://doi.org/10.1016/0037-0738(79)90072-1.
- Allen, P.A., Cabrera, L., Colombo, F., Matter, A., 1983. Variations in fluvial style on the eocene—oligocene alluvial fan of the scala dei group, SE ebro basin, Spain. J. Geol. Soc. 140 (1), 133–146. https://doi.org/10.1144/gsjgs.140.1.0133.
- Amajor, L.C., Agbaire, D.W., 1989. Depositional history of the reservoir sandstones, Akpor and Apara oilfields, eastern Niger Delta, Nigeria. J. Petrol. Geol. 12 (4), 453–464. https://doi.org/10.1111/j.1747-5457.1989.tb00243.x.
- Asquith B., George, 1982. Basic Well Log Analysis for Geologists. American Association of Petroleum Geologists. https://doi.org/10.1306/mth3425c6.
- Bernabé, Y., Li, M., Maineult, A., 2010. Permeability and pore connectivity: a new model based on network simulations. J. Geophys. Res. Solid Earth 115 (B10). https://doi.org/10.1029/2010JB007444.
- Bridge, J.S., Mackey, S.D., 1993. A Revised Alluvial Stratigraphy Model. Alluvial sedimentation, pp. 317–336. https://doi.org/10.1002/9781444303995.ch22.
- Bridge, J.S., 1993. The interaction between channel geometry, water flow, sediment transport and deposition in braided rivers. Geological Society, London, Special Publications 75 (1), 13–71. https://doi.org/10.1144/GSLSP.1993.075.01.02.
- Bridge, J.S., Tye, R.S., 2000. Interpreting the dimensions of ancient fluvial channel bars, channels, and channel belts from wireline-logs and cores. AAPG Bull. 84 (8), 1205–1228. https://doi.org/10.1306/A9673C84-1738-11D7-8645000102C1865D.
- Cai, J., Zhang, Z., Wei, W., Guo, D., Li, S., Zhao, P., 2019. The critical factors for permeability-formation factor relation in reservoir rocks: pore-throat ratio, tortuosity and connectivity. Energy 188, 116051. https://doi.org/10.1016/ j.energy.2019.116051.
- Cant, R.V., 1992. Geological implications of deep well disposal in the Bahamas. In: Natural Hazards in the Caribbean, pp. 66–73.
- Charvin, K., Hampson, G.J., Gallagher, K.L., Storms, J.E., Labourdette, R., 2011. Characterization of controls on high-resolution stratigraphic architecture in wave-dominated shoreface—shelf parasequences using inverse numerical modeling. J. Sediment. Res. 81 (8), 562–578. https://doi.org/10.2110/jsr.2011.48.
- Chow, J.J., Ming-Chung, L., Fuh, S.C., 2005. Geophysical well log study on the paleoenvironment of the hydrocarbon producing zones in the Erchungchi Formation, Hsinyin, SW Taiwan. TAO: Terr. Atmos. Ocean Sci. 16 (3), 531. https://doi.org/10.3319/tao.2005.16.3.531(t.
- Corbett, M.J., Fielding, C.R., Birgenheier, L.P., 2011. Stratigraphy of a cretaceous coastal-plain fluvial succession: the campanian masuk formation, henry

- mountains syncline, Utah, USA. J. Sediment. Res. 81 (2), 80–96. https://doi.org/10.2110/isr.2011.12.
- Crossley, A.R., 1990. The Geology and Hydrocarbon Potential of the Pattani Basin Gulf of Thailand-An Overview-: Unocal Thailand Internal Report.
- Durkin, P.R., Boyd, R.L., Hubbard, S.M., Shultz, A.W., Blum, M.D., 2017. Three-dimensional reconstruction of meander-belt evolution, Cretaceous McMurray Formation, Alberta foreland basin, Canada. J. Sediment. Res. 87 (10), 1075–1099. https://doi.org/10.2110/jsr.2017.59.
- Fielding, C.R., Crane, R.C., 1987. An application of statistical modelling to the prediction of hydrocarbon recovery factors in fluvial reservoir sequences. Special Publications of SEPM 39, 321–327. https://doi.org/10.2110/pec.87.39.0321.
- Hajek, E.A., Heller, P.L., Sheets, B.A., 2010. Significance of channel-belt clustering in alluvial basins. Geology 38 (6), 535–538. https://doi.org/10.1130/G30783.1.
- Heldreich, G., Redfern, J., Legler, B., Gerdes, K., Williams, B.P.J., 2017. Challenges in characterizing subsurface paralic reservoir geometries: a detailed case study of the Mungaroo Formation, North West Shelf, Australia. Geological Society, London, Special Publications 444 (1), 59–108. https://doi.org/10.1144/SP444.13.
- Hornung, J., Aigner, T., 1999. Reservoir and aquifer characterization of fluvial architectural elements: stubensandstein, Upper Triassic, southwest Germany. Sediment. Geol. 129 (3–4), 215–280. https://doi.org/10.1016/S0037-0738(99) 00103-7.
- Hossain, S., 2018. Seismic geomorphology as a tool for reservoir characterization: a case study from Moragot field of Pattani Basin, Gulf of Thailand. Malays. J. Geosci. (MJG). 3 (1), 45–50. https://doi.org/10.26480/mjg.01.2019.45.50.
- Hubbard, S.M., Smith, D.G., Nielsen, H., Leckie, D.A., Fustic, M., Spencer, R.J., Bloom, L., 2011. Seismic geomorphology and sedimentology of a tidally influenced river deposit, Lower Cretaceous Athabasca oil sands, Alberta, Canada. AAPG Bull. 95 (7), 1123–1145. https://doi.org/10.1306/12131010111.
- Imran, Q.S., Siddiqui, N.A., Latif, A.H.A., Bashir, Y., Ali, A.A.A.S., Jamil, M., 2020. Integrated well data and 3D seismic inversion study for reservoir delineation and description. Bull. Geol. Soc. Malays. 70, 209–220. https://doi.org/10.7186/bgsm70202016.
- Jackson, P.D., Smith, D.T., Stanford, P.N., 1978. Resistivity-porosity-particle shape relationships for marine sands. Geophysics 43 (6), 1250–1268. https://doi.org/ 10.1190/1.1440891.
- Jardine, E., 1997. Dual petroleum systems governing the prolific Pattani Basin, offshore Thailand. Proceedings of an International Conference on Petroleum Systems of SE Asia and Australasia. https://doi.org/10.29118/ipa.87.351.363.
- Kessler, L.G., Sachs, S.D., 1995. Depositional setting and sequence stratigraphic implications of the upper sinemurian (lower jurassic) sandstone interval, north celtic sea/st george's channel basins, offshore Ireland. Geological Society, London, Special Publications 93 (1), 171–192. https://doi.org/10.1144/ GSL.SP.1995.093.01.13.
- Kongwung, B., Ronghe, S., 2000. Reservoir identification and characterization through sequential horizon mapping and geostatistical analysis: a case study from the Gulf of Thailand. Petrol. Geosci. 6 (1), 47–57. https://doi.org/10.1144/petgeo.6.1.47.
- Lambiase, J., Narapan, J., Champasa, P., 2016. Marginal marine Mudstones in the Pattani basin, gulf of Thailand: implications for Stratigraphic development, reservoir characterization and correlation potential. Implications for Stratigraphic development, reservoir characterization and correlation potential Barcelona, Spain. In: International Conference and Exhibition, pp. 3–6. https:// doi.org/10.1190/ice2016-6314635.1.
- Larue, D.K., Hovadik, J., 2006. Connectivity of channelized reservoirs: a modelling approach. Petrol. Geosci. 12 (4), 291–308. https://doi.org/10.1144/1354-079306-699.
- Leeder, M.R., 1973. Fluviatile fining-upwards cycles and the magnitude of palae-ochannels. Geol. Mag. 110 (3), 265–276. https://doi.org/10.1017/S0016756800036098.
- Li, S., Xiao, T., Zheng, B., 2012. Medical geology of arsenic, selenium and thallium in China. Sci. Total Environ. 421, 31—40. https://doi.org/10.1016/j.scitotenv.2011.02.040.
- Lorenz, J.C., Heinze, D.M., Clark, J.A., Searls, C.A., 1985. Determination of widths of meander-belt sandstone reservoirs from vertical downhole data, Mesaverde Group, Piceance Creek Basin, Colorado. AAPG Bull. 69 (5), 710–721. https:// doi.org/10.1306/AD4627EF-16F7-11D7-8645000102C1865D.
- Lundegard, P.D., Trevena, A.S., 1990. Sandstone diagenesis in the Pattani Basin (Gulf of Thailand): history of water-rock interaction and comparison with the Gulf of Mexico. Appl. Geochem. 5 (5–6), 669–685. https://doi.org/10.1016/0883-2927(90)90064-C.
- Magoba, M., Opuwari, M., 2020. Petrophysical interpretation and fluid substitution modelling of the upper shallow marine sandstone reservoirs in the Bredasdorp Basin, offshore South Africa. J. Pet. Explor. Prod. Technol. 10 (2), 783–803. https://doi.org/10.1007/s13202-019-00796-1.
- Miall, A.D., 2002. Architecture and sequence stratigraphy of Pleistocene fluvial systems in the Malay Basin, based on seismic time-slice analysis. AAPG Bull. 86 (7), 1201–1216. https://doi.org/10.1306/61EEDC56-173E-11D7-8645000102C1865D.
- Mondol, N.H., 2015. Well logging: principles, applications and uncertainties. In: Petroleum Geoscience. Springer, Berlin, Heidelberg, pp. 385–425. https://doi.org/10.1007/978-3-642-34132-8_16.
- Morley, C.K., 2013. Discussion of tectonic models for Cenozoic strike-slip fault-affected continental margins of mainland SE Asia. J. Asian Earth Sci. 76, 137–151. https://doi.org/10.1016/j.jseaes.2012.10.019.
- Mountford, A.S., Morales Maqueda, M.A., 2019. Eulerian Modeling of the three-

- dimensional distribution of seven popular microplastic types in the global ocean. J. Geophys. Res.: Oceans 124 (12), 8558–8573. https://doi.org/10.1029/2019IC015050.
- Nazeer, Å., Abbasi, S.A., Solangi, S.H., 2016. Sedimentary facies interpretation of gamma ray (GR) log as basic well logs in central and lower indus basin of Pakistan. Geodesy Geodyn. 7 (6), 432–443. https://doi.org/10.1016/i.geog.2016.06.006.
- Onyekuru, S.O., Ibelegbu, E.C., Iwuagwu, J.C., Essien, A.G., Akaolisa, C.Z., 2012. Sequence stratigraphic analysis of "XB field,". Central Swamp Depobelt, Niger Delta Basin, Cent. Swamp Niger Delta Basin South. Niger. Int. J. Geosci. International Journal of Geosciences 3 (1), 237. https://doi.org/10.4236/iig.2012.31027.
- Opuwari, M., Bialik, O.M., Taha, N., Waldmann, N.D., 2021. The role of detrital components in the petrophysical parameters of Paleogene calcareousdominated hemipelagic deposits. Arabian J. Geosci. 14 (11), 1–13. https:// doi.org/10.1007/s12517-021-07328-4.
- Polachan, S., Pradidtan, S., Tongtaow, C., Janmaha, S., Intarawijitr, K., Sangsuwan, C., 1991. Development of cenozoic basins in Thailand. Mar. Petrol. Geol. 8 (1), 84–97. https://doi.org/10.1016/0264-8172(91)90047-5.
- Potter, P.E., 1967. Sand bodies and sedimentary environments: a review. AAPG (Am. Assoc. Pet. Geol.) Bull. 51 (3), 337–365. https://doi.org/10.1306/5d25b7e5-16c1-11d7-8645000102c1865d.
- Pupon, Andre, Leveaux, J., 1971. Evaluation Of Water Saturation In Shaly Formations. SPWLA 12th Annual Logging Symposium.
- Rafaelsen, B., 2006. Seismic Resolution and Frequency Filtering. Univ. Tromso Lecture Series. Tromso. Norway.
- Raiber, M., White, P.A., Daughney, C.J., Tschritter, C., Davidson, P., Bainbridge, S.E., 2012. Three-dimensional geological modelling and multivariate statistical analysis of water chemistry data to analyse and visualise aquifer structure and groundwater composition in the Wairau Plain, Marlborough District, New Zealand. J. Hydrol. 436, 13–34. https://doi.org/10.1016/ji.jhydrol.2012.01.045.
- Reijenstein, H.M., Posamentier, H.W., Bhattacharya, J.P., 2011. Seismic geomorphology and high-resolution seismic stratigraphy of inner-shelf fluvial, estuarine, deltaic, and marine sequences, Gulf of ThailandSeismic Geomorphology and Stratigraphy in the Gulf of Thailand. AAPG Bull. 95 (11), 1959–1990. https://doi.org/10.1306/03151110134.
- Richards, Keller, 1982. Rivers: form and process in alluvial channels. SAGE 9 (1). https://doi.org/10.1177/030913338500900111.
- Rider, M., 1996. The Geological Interpretation of Well Logs. John Wiley and Sons, Inc, New York, NY (USA), ISBN 0-470-20281-5, p. 192, 1986.
- Salem, H.S., Chilingarian, G.V., 1999. The cementation factor of Archie's equation for shaly sandstone reservoirs. J. Petrol. Sci. Eng. 23 (2), 83–93. https://doi.org/ 10.1016/S0920-4105(99)00009-1.
- Selley, R.C., Sonnenberg, S.A., 1985. Methods of exploration. Elem. Petrol. Geol.

- 43-166. https://doi.org/10.1016/b978-0-12-822316-1.00003-3.
- Shanley, K.W., 2004. Fluvial Reservoir Description for a Giant, Low-Permeability Gas Field: Jonah Field. Green River Basin, Wyoming, USA. https://doi.org/10.1306/ st521007.
- Straub, K.M., Paola, C., Mohrig, D., Wolinsky, M.A., George, T., 2009. Compensational stacking of channelized sedimentary deposits. J. Sediment. Res. 79 (9), 673–688. https://doi.org/10.2110/jsr.2009.070.
- Tiab, D., Donaldson, E.C., 2015. Chapter 3: porosity and permeability. Petrophysics. In: Theory and Practice of Measuring Reservoir Rock and Fluid Transport Properties, fourth ed. Elsevier. https://doi.org/10.1016/B978-0-12-803188-9.00003-6.
- Timur, A., 1968. An investigation of permeability, porosity, and residual water saturation relationships. SPWLA 9th Annual Logging Symposium. OnePetro. https://doi.org/10.1088/1742-6596/106/1/012004.
- Usman, M., Siddiqui, N.A., Mathew, M., Zhang, S., El-Ghali, M.A., Ramkumar, M., Jamil, M., Zhang, Y., 2020. Linking the influence of diagenetic properties and clay texture on reservoir quality in sandstones from NW Borneo. Mar. Petrol. Geol. 120, 104509. https://doi.org/10.1016/j.marpetgeo.2020.104509.
- Geol. 120, 104509. https://doi.org/10.1016/j.marpetgeo.2020.104509.

 Verwer, K., Eberli, G.P., Weger, R.J., 2011. Effect of pore structure on electrical resistivity in carbonates. AAPG Bull. 95 (2), 175–190. https://doi.org/10.1306/06301010047.
- Williams, G.P., 1986. River meanders and channel size. J. Hydrol. 88 (1–2), 147–164. https://doi.org/10.1016/0022-1694(86)90202-7.
- Worthington, P.F. 1988. Conjunctive interpretation of core and log data through association of effective and total porosity models. Geol. Soc. Lond. 136 (1), 213–223. https://doi.org/10.1144/gsl.sp.1998.136.01.18.

 Wu, C., Bhattacharya, J.P., Ullah, M.S., 2015. Paleohydrology and 3D facies archi-
- Wu, C., Bhattacharya, J.P., Ullah, M.S., 2015. Paleohydrology and 3D facies architecture of ancient point bars, ferron sandstone, notom delta, south-central Utah, us Apaleohydrology and 3D facies architecture of ancient point bars. J. Sediment. Res. 85 (4), 399–418. https://doi.org/10.2110/jsr.2015.29.
- Willis, Zha, Willis, B.J., 1989. Palaeochannel reconstructions from point bar deposits: a three-dimensional perspective. Sedimentology 36 (5), 757–766. https://doi.org/10.1111/j.1365-3091.1989.tb01744.x, 1989.
 Zhang, F., Xiao, H., Jiang, Z., Tang, X., Liu, X., Guo, H., Zhao, W., Zhu, L., Li, X., Zhan, S.,
- Zhang, F., Xiao, H., Jiang, Z., Tang, X., Liu, X., Guo, H., Zhao, W., Zhu, L., Li, X., Zhan, S., 2021. Influence of pore throat structure and the multiphases fluid seepage on mobility of tight oil reservoir. Lithosphere 1–18. https://doi.org/10.2113/2021/ 5525670.
- Zheng, S.Y., Corbett, P.W.M., Emery, A., 2003. Geological interpretation of well test analysis: a case study from a fluvial reservoir in the Gulf of Thailand. J. Petrol. Geol. 26 (1), 49–64. https://doi.org/10.1111/j.1747-5457.2003.tb00017.x.
- Zou, C., Dong, D., Wang, S., Li, J., Li, X., Wang, Y., Li, D., Cheng, K., 2010. Geological characteristics and resource potential of shale gas in China. Petrol. Explor. Dev. 37 (6), 641–653. https://doi.org/10.1016/S1876-3804(11)60001-3.